International Journal of Nanomedicine

Dovepress
Taylor & Francis Group

Open Access Full Text Article

ORIGINAL RESEARCH

Micro-Electro Nanofibrous Dressings Based on PVDF-AgNPs as Wound Healing Materials to Promote Healing in Active Areas

Tiantian Liu[1,2,*], Feifei Xie[3,4,*], Lele Geng[1,2], Ruizhe He[1,2], Mengzhe Sun[1,2], Tao Ni[1,2], Peng Xu[1,2], Chao Xing[1,2], Yinbo Peng[1,2], Ke Chen[3,4], Yong Fang[1,2]

[1]Department of Burns and Plastic Surgery, Shanghai Ninth People's Hospital, Shanghai Jiao Tong University School of Medicine, Shanghai, People's Republic of China; [2]Institute of Traumatic Medicine, Shanghai Jiao Tong University School of Medicine, Shanghai, People's Republic of China; [3]School of Materials Science and Engineering, Shanghai Jiao Tong University, Shanghai, People's Republic of China; [4]Shanghai Key Laboratory of Materials Laser Processing and Modification, Shanghai Jiao Tong University, Shanghai, People's Republic of China

*These authors contributed equally to this work

Correspondence: Yong Fang, Department of Burns and Plastic Surgery, Shanghai Ninth People's Hospital, Shanghai Jiao Tong University School of Medicine, Shanghai, People's Republic of China, Email fangyong1020@hotmail.com; Ke Chen, School of Materials Science and Engineering, Shanghai Jiao Tong University, Shanghai, People's Republic of China, Email chenke83@sjtu.edu.cn

Purpose: The purpose of this study is to develop an innovative solution for chronic wounds in high-mobility areas, such as joints, where conventional treatments are hindered by passive healing mechanisms and the need for immobilization. By designing a micro-electro-Nanofiber dressing composed of piezoelectric polyvinylidene fluoride (PVDF) integrated with antimicrobial silver nanoparticles (AgNPs), this research aims to address the dual challenges of promoting effective wound healing and maintaining joint mobility.

Methods: Herein, we developed a novel micro-electro-Nanofiber dressing using electrospinning technology, incorporating polyvinylidene fluoride (PVDF) with silver nanoparticles (AgNPs). The optimized PVDF-AgNPs Nanofiber dressings exhibited strong piezoelectric effects suitable for joint wounds.

Results: In vitro experiments demonstrated that the dressing effectively promoted fibroblast migration and collagen synthesis. In vivo, the dressing exhibited a trend of rapid healing in infected wounds within 12 days while modulating macrophage differentiation toward the anti-inflammatory M2 phenotype. Additionally, the incorporation of antimicrobial nanosilver effectively controlled local infections, further facilitating the healing process.

Conclusion: To sum up, by harnessing the piezoelectric effect to stimulate endogenous healing mechanisms without restricting joint mobility, the developed PVDF-AgNPs Nanofiber dressings represent a transformative approach for the treatment of wounds in highly mobile body areas.

Keywords: wound healing, piezoelectric materials, polyvinylidene fluoride, silver nanoparticles

Introduction

When chronic wounds are located in areas with high mobility, such as joints, the continuous mechanical stretching of the wounds will result in a perpetual cycle of healing, disruption, and re-healing, which delays recovery and may even lead to complications such as hypertrophic scarring.[1–3] This type of wound healing presents a particularly challenging clinical problem. To address this issue, current wound healing models recommend limiting activity at the injury site to prevent delays in healing caused by surrounding tissue tension.[4] However, prolonged local immobilization can lead to complications for patients, including muscle atrophy, limited joint mobility, and even thrombosis and pressure ulcers, ultimately resulting in local scarring, tissue contraction, and decreased bone density.[5–7] Therefore, it is crucial in clinical treatment to develop a therapeutic approach that promotes wound healing at joint sites without restricting joint mobility, thus accelerating the patient's recovery of autonomous activity, reducing complications, and restoring social capabilities.

Received: 14 November 2024
Accepted: 9 January 2025
Published: 18 January 2025

Graphical Abstract

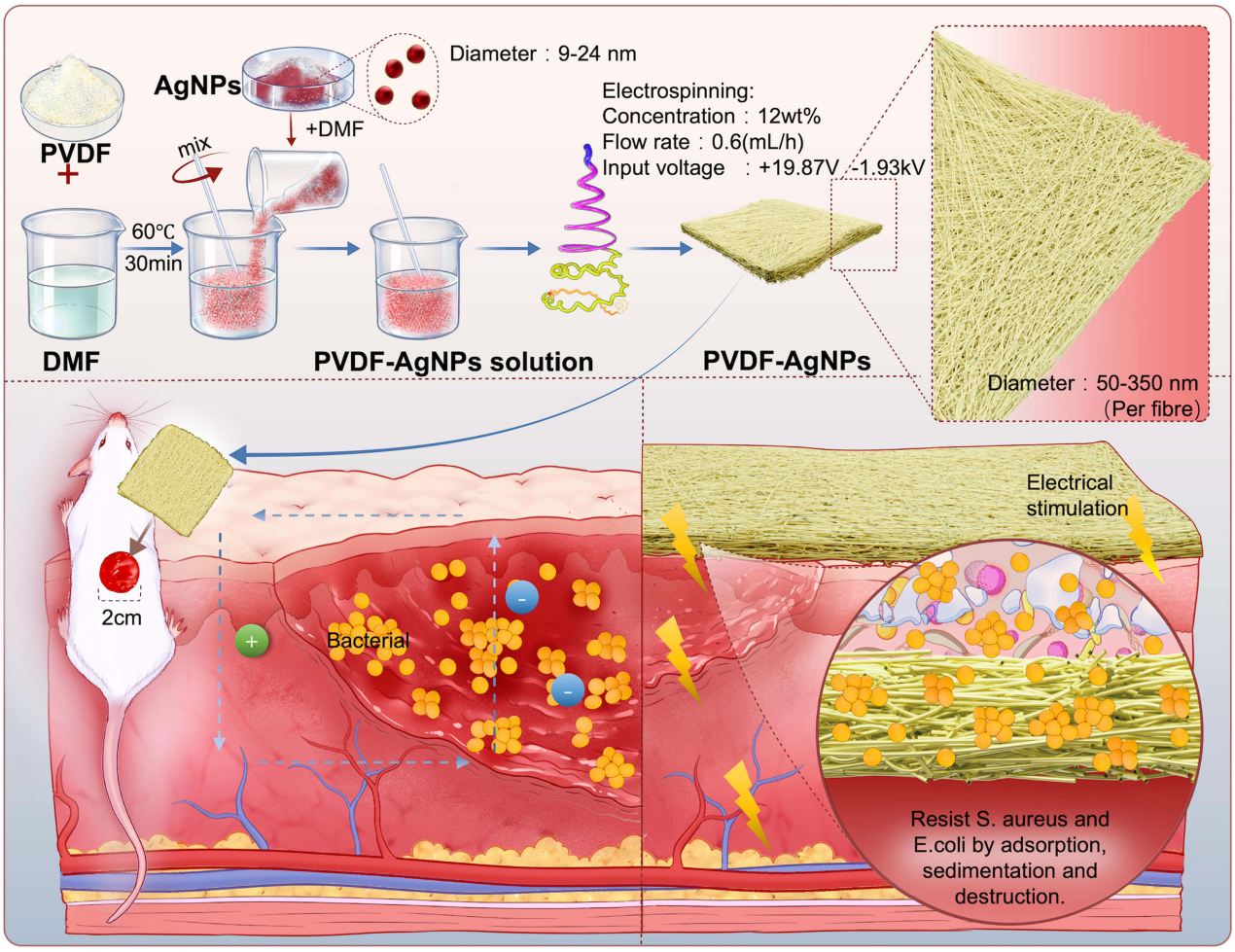

To address both the healing and mobility needs of joint wounds, various dressings such as elastic hydrogels,[8–10] anti-wrinkle hydrogels,[11,12] or high-viscosity hydrogel dressings are typically employed.[13–15] For example, alginate-based helical fibers incorporated into polyacrylamide/gelatin (PAM-Gel) create hydrogel dressings with high elastic mechanical properties that effectively adapt to the movement of joint wounds.[9] Additionally, the combination of electrospinning technology and water-induced self-assembly methods has been used to produce biomimetic conductive dressings with arranged wrinkles. For instance, γ-PGA/PEG-NH2 hydrogels not only form covalent amide bonds with biological tissue surfaces to achieve strong wet adhesion but also establish a stable chemical crosslinking network within the volumetric hydrogel to resist deformation.[8] Despite these advancements, the aforementioned joint wound healing dressings are passive and do not actively stimulate endogenous cells for wound healing and the healing cycle still requires improvement. To further overcome these challenges, various kinds of physiotherapy have been developed, including but not limited to electricity, ultrasound, heat and magnetic field, etc. Among these electric has been proven efficient in regulating cell proliferation and migration, reducing inflammation, and accelerating wound bed closure.[16–18] Besides, due to the urgent demands for personalized and point-of-care programs, portable self-powered devices have been proposed, providing new insights for promoting wound healing through electrical stimulation. In addition, because piezoelectric materials can generate electric fields even under small mechanical deformation, they hold great potential to

be used as a self-powered dressing for joint healing without a subsidiary.[19,20] However, current research on creating joint wound repair materials using the spontaneous discharge properties of piezoelectric materials is virtually non-existent.

To bridge these gaps, this study introduces a novel piezoelectric dressing concept that integrates the spontaneous discharge properties of piezoelectric materials with antimicrobial functionality and personalized adaptability. Unlike conventional joint wound dressings, our approach leverages electrospinning technology to fabricate micro-electro-Nanofiber dressings composed of polyvinylidene fluoride (PVDF) and silver nanoparticles (AgNPs), creating a flexible and highly responsive material capable of promoting wound healing in high-mobility regions. Piezoelectric materials, such as PVDF, stand out due to their unique ability to generate an electric field under mechanical deformation, promoting cellular activities such as proliferation, migration, and collagen synthesis. Compared to other piezoelectric materials, PVDF offers a combination of high flexibility, excellent biocompatibility, and processability, making it particularly suitable for dynamic wound environments like joints. Silver nanoparticles (AgNPs) have long been recognized for their potent antimicrobial properties, effectively controlling infections without the risk of antibiotic resistance. When integrated with PVDF, AgNPs not only enhance the antimicrobial efficacy of the dressing but also contribute to the material's overall mechanical stability. This dual-functional synergy is challenging to achieve with conventional materials like hydrogels or elastomers.By precisely controlling process parameters such as PVDF concentration, Ag/PVDF mass ratio, and solution flow rate, we have further optimized the conditions to create the most suitable joint wound piezoelectric dressings. Both in vitro and in vivo studies confirm that these Nanofiber dressings are highly biocompatible, promoting fibroblast migration, collagen deposition, and re-epithelialization, thus significantly accelerating wound healing. The addition of nanosilver provides potent antimicrobial protection, effectively controlling local wound infections and promoting the healing of infectious wounds. In vivo experiments show that PVDF-AgNPs dressings facilitate a rapid healing trend of infected wounds within 12 days while regulating macrophage differentiation in skin tissues towards the anti-inflammatory M2 phenotype. Overall, these PVDF-AgNPs Nanofiber dressings can serve as personalized "energy skin" for highly active joint wounds, balancing high mobility and healing promotion, and opening up their clinical application prospects in modern wound treatment.

Material and Methods

Materials and Equipment

Materials

Polyvinylidene fluoride (PVDF) was purchased from Bidepharm (Shanghai, China). N, N-Dimethylformamide (DMF, ACS spectroscopic grade, ≥ 99.8%) was acquired from Aladdin (Shanghai, China). Silver nanoparticles (AgNPs, ≥ 99.99%) powder was obtained from HUZHENG. Nitric acid (CMOS grade) was sourced from China National Pharmaceutical Group Chemical Reagent Co., Ltd. Human dermal fibroblasts (HDF, Shanghai Yubo Biotechnology Co., Ltd., YB-ATCC-9221, Shanghai, China) used in this study were obtained from American Type Culture Collection (ATCC), passage numbers ranging from P5 to P6. Ethanol, crystal violet, glutaraldehyde, phosphate-buffered saline (PBS, PH 7.2), fetal bovine serum (FBS, 10%), and the Cell Counting Kit-8 (CCK-8) were all obtained from Merck Sigma-Aldrich (Shanghai, China). Paraffin embedding medium was purchased from China National Pharmaceutical Group Chemical Reagent Co., Ltd (Shanghai, China). BD Falcon 24-well tissue culture plates were obtained from Fisher Scientific (Shanghai, China). Rainin pipette tips (1 mL) were sourced from Mettler-Toledo (Shanghai, China). PP centrifuge tubes were acquired from CNW and ANPEL Laboratory Technologies (Shanghai, China) Inc. Anti-CD206 antibody was purchased from SantaCruz (Shanghai, China). Rat TNF-alpha ELISA Kit (ab236712), Rat IFN-gamma ELISA Kit (ab239425), Rat IL-6 ELISA Kit (ab234570), Rat IL-10 ELISA Kit (ab214566), Anti-CD68 antibody (ab283654), Anti-CD86 antibody (ab238468), and Anti-Mannose Receptor antibody (ab64693) were all obtained from Abcam (Shanghai, China).

Equipment

Electrospinning machine (Laboratory of the School of Materials Science and Engineering, Shanghai Jiao Tong University, Shanghai, China). Scanning Electron Microscope (SEM, Sirion 200) was sourced from FEI NanoPorts (Shanghai, China). ATR-FTIR (Nicolet 6700) was obtained from Thermo Scientific (Shanghai, China). X-ray

Diffraction (XRD, D8 DaVinci) was purchased from Bruker (Shanghai, China). Differential Scanning Calorimetry (DSC, Q20) was sourced from TA Instruments (Dongguan, China). Atomic Force Microscopes (AFM, MFP-3D) were obtained from Oxford Instruments and AFM (FastScan Bio) from Bruker (Shanghai, China). The graphite digestion furnace (DigiPREP LS) was sourced from SCE SCIENCE. Inductively Coupled Plasma Optical Emission Spectroscopy (ICAP 7600) was obtained from Thermo Fisher (Analysis and Testing Center of Shanghai Jiao Tong University, Shanghai, China). Fluorescence microscopy observations were conducted using a Soptop ICX 41 from Sunny Optical Technology Co., Ltd. (Hong Kong, China). Transmission Electron Microscope/Energy Dispersive Spectroscopy (TEM-EDS) was sourced from JEOL JEM F200 and Tecnai G2 F30 (Laboratory of the School of Materials Science and Engineering, Shanghai Jiao Tong University, Shanghai, China).

Methods

Electrospinning Design and Preparation of Fiber Dressings

The preparation process involves material dissolution and electrospinning (Table 1). PVDF powder and DMF are measured, creating a 12% w/v PVDF/DMF solution in a beaker, stirred at 60°C with a water bath magnetic stirrer until fully dissolved. For silver incorporation, AgNP powder is dissolved in 1 mL of DMF and added to the PVDF solution, stirring until a homogeneous mixture is achieved, maintaining the PVDF/DMF mass fraction.To minimize variable influences, we standardized the electrospinning machine's environment and parameters. The needle distance was selected based on fixed endpoints for synchronized rotation, enhancing efficiency. To maximize fiber polarization, we applied the device's maximum voltage. The "heating" fan was activated approximately 2 hours prior to electrospinning to stabilize system operation. Literature indicates higher rotation speeds produce more orderly fiber arrangements;[21,22] thus, we chose a high rotation speed for material collection and fixation. PVDF provides piezoelectric performance, while AgNPs function as the primary antibacterial agent and boost piezoelectric properties, yielding PVDF-AgNP nanofiber dressings with superior piezoelectric and antibacterial qualities.[23] A needleless syringe is used to slowly withdraw the solution, preventing bubbles. An 18-gauge syringe needle, fixed to the positive electrode, serves as the spinneret, with a grounded collector roller 12 cm away, rotating at 1500 rpm. A soft surface rotor, positioned 10 cm from the metal needle, collects PVDF-AgNPs piezoelectric nanofibers at a uniform speed. Before electrospinning, proper solution flow through the conduit is confirmed to prevent electrical leakage. For safety, the voltage is set to +19.87 kV and −1.93 kV (Figure S1).

Characterization of Fiber Dressings

To identify the three common phases of PVDF (α, β, γ), we employed ATR-FTIR, XRD, and DSC for comprehensive evaluation and optimal formulation selection. The purpose of ATR-FTIR analysis was to identify the characteristic vibrational modes of PVDF phases, particularly the β-phase, which is critical for piezoelectric properties. XRD was used to confirm the crystalline phases and quantify the β-phase fraction, while DSC provided thermal characterization to evaluate phase transitions and crystallinity. AFM measured displacement and electric potential for piezoelectric

Table 1 Parameter Settings are Outlined in Table 1, Including PVDF Concentration, Silver Amount, Flow Rate, Temperature, and Humidity

Group	Concentration (wt%)	Mass Ratio of Ag/PVDF	Flow Rate (mL/h)	Temperature (°C)	Humidity (%)
1	12	0	0.6	32.6–34.2	10–13
2	12	0.05/6	0.6	32.3–35.1	10–15
3	12	0.1/6	0.6	32.7–33.3	10–12
4	12	0.2/6	0.6	31.8–34.3	10–14
5	12	0.4/6	0.6	31.8–32.7	11–13
6	12	0.8/6	0.6	31.0–32.3	12–15

characterization, providing insights into the material's electrical responsiveness. Scanning Electron Microscopy (SEM) observed film morphology to analyze fiber uniformity and structure, and ImageJ quantified fiber diameter distribution to ensure consistency and optimize electrospinning parameters.

Vitro Experiments

Silver Release and Antibacterial Testing: We assessed antibacterial stability and silver release by placing five materials in sterile broth (10 mL, 36°C) with 60 μg/mL silver ion concentration. At set intervals, 3 mL samples were extracted and replaced to maintain agitation. For antibacterial assays, Escherichia coli (E. coli) and Staphylococcus aureus (S. aureus) solutions (10^5 cells) were prepared, and five material masses were added according to silver ion concentration, with a control group. Samples at 0 h, 2 h, 4 h, and 12 h were analyzed by ICP-OES (iCAP 7600), and SEM/TEM-EDS observed bacterial morphology after 12 h.

Cell Biocompatibility Evaluation: Fiber dressings were UV-sterilized, immersed in cell culture medium, and extracts incubated with HDF cells for 24 and 48 hours. Cell viability was measured using the CCK-8 assay. Cytotoxicity was evaluated through live/dead cell staining and observed under fluorescence microscopy. Fluorescence microscopy was conducted using a Soptop ICX 41 (Sunny Optical Technology Co., Ltd)., with excitation/emission wavelengths set at 494/517 nm for Calcein-AM and 535/617 nm for PI. Images were observed and captured at 10× and 20× magnifications. Fluorescence intensity was quantified using ImageJ software to ensure result accuracy.

Scratch Wound Healing Assay: HDF cells in DMEM with 10% FBS were scratched to create a cross-hatch wound pattern in a 24-well plate. Wells were treated with extracts from fiber dressings, and materials were placed over wells. Pull tests were conducted every 2 hours over 24 hours to observe cell migration and proliferation, with six repetitions per group.

In vivo Experiments

Establishment of *S. aureus*-Infected Skin Defect Model in Rats and Wound Healing Observation: Animal experiments were approved by the Animal Protection Committee of the Ninth People's Hospital, Shanghai Jiao Tong University (Approval: SH9H-2019-A704-1). All procedures were conducted in strict accordance with the National Institutes of Health (NIH) Guide for the Care and Use of Animals in laboratory experiments.

A clinical *S. aureus* isolate was cultured, and 8–10-week-old male Sprague-Dawley rats were housed under controlled conditions. After a 10-day acclimation period, the rats' backs were shaved, and full-thickness skin wounds were created. The wounds were infected with S. aureus and treated in the following four groups: Gauze (control group); Gauze with AgNPs; PVDF fiber dressing; PVDF-AgNPs dressing.Wound healing was monitored by measuring closure rates and capturing images up to Day 12. The healing rate was calculated using the formula:

$$(S - St)/S \times 100\%.$$

HE Staining: Skin samples were fixed, deparaffinized, and stained using hematoxylin-eosin (HE) to assess cell nuclei and tissue structure.

Masson Staining: Tissues were deparaffinized and stained with Masson's trichrome to analyze collagen distribution.

Immunofluorescence Analysis: CD68, CD86, and CD206 co-staining immunofluorescence was performed as follows: sections were deparaffinized, underwent antigen retrieval, and were incubated with primary and secondary antibodies, followed by DAPI staining for fluorescence microscopy using a Soptop ICX 41 (Sunny Optical Technology Co., Ltd). The excitation/emission wavelengths were set at 488/517 nm for Alexa Fluor 488 (green fluorescence), 594/617 nm for Alexa Fluor 594 (red fluorescence), and 358/461 nm for DAPI (blue fluorescence). Fluorescence intensity was quantified using ImageJ software.

ELISA Analysis: On Days 3, 6, 9, and 12, skin tissue homogenates were centrifuged, and the supernatants were collected for analysis. Samples were prepared in enzyme-labeled plates, incubated, and absorbance was measured at 450 nm. Statistical analysis was performed afterward.

Statistical Analysis

All data are presented as mean ± standard deviation (SD), and statistical significance was calculated using GraphPad Prism 9.0 (Graph-Pad Software, CA, USA). The *t*-test or analysis of variance (ANOVA) was used to determine statistical

significance. A P-value of less than 0.05 was considered significant. The results of significant differences were indicated as follows: ns: no statistical difference; *: $P < 0.05$; **: $P < 0.01$; ***: $P < 0.005$; ****: $P < 0.001$.

Results

Electrospinning Design, Preparation, and Characterization of Fiber Dressings

Considering the molecular weight and the constraints of the electrospinning machine, we chose 12 wt% and a flow rate of 0.6 mL/h for further studies.[21,24] Additionally, the amount of AgNPs added to the system can alter the sample's conductivity, interaction forces with dipoles, as well as biocompatibility and antibacterial effects. We set five mass ratios of AgNPs to PVDF: 0.05/6, 0.1/6, 0.2/6, 0.4/6, and 0.8/6 to identify suitable ranges for antibacterial effects and biocompatibility.

We used SEM to characterize the morphology of PVDF-AgNPs fiber surfaces, as SEM is highly sensitive to changes in shape and height. Additionally, the arrangement of the fiber materials can be visually observed at different magnifications: lower magnification shows the overall condition of the sample, while higher magnification provides more details. With the help of ImageJ, we measured the fiber diameter and determined the size distribution.

As shown in Figure 1A, PVDF-AgNPs fibers electrospun from 12 wt% PVDF at a flow rate of 0.6 mL/h, with varying mass ratios of AgNPs/PVDF: Pure (pure PVDF film), 0.05/6, 0.1/6, 0.2/6, 0.4/6, and 0.8/6. The Pure group showed lower conductivity due to lack of silver nanoparticles, leading to uneven spin and beaded fiber. In contrast, the fibers in silver-containing films were relatively uniform in diameter, with a reduced number of beads. The diameter distribution patterns of silver-containing films were different, but the ranges were similar. Furthermore, the increased in silver content was independent of fiber diameter. The average fiber diameters for the groups Pure (pure PVDF film), 0.05/6, 0.1/6, 0.2/6, 0.4/6, and 0.8/6 were collected and showed in Figure 1Bi–1Bvii (pure: 127.61±65.40 μm; 0.05/6: 178.94±56.70 μm; 0.1/6: 167.25±78.42 μm; 0.2/6: 164.94±75.75 μm; 0.4/6: 131.09±55.33 μm; 0.8/6: 214.89±96.37 μm), respectively. The fiber diameter distribution primarily ranged from 50 to 100 nm, with fiber quantity decreasing as the diameter increased. Comparing Figure 1Bvii, we found that the average diameters for AgNPs/PVDF ratios of 0.1/6 and 0.2/6 were similar, while the sample with a mass ratio of 0.8/6 exhibited a larger average diameter, consistent with the relationship between average diameter and dispersion. However, the fiber diameter distribution for 0.1/6 was uneven, with the greatest variance in fiber diameters and lower precision; the distributions for 0.05/6 and 0.2/6 were more uniform (Figure S2a), with approximately 80% of fiber diameters at 200 nm. Previous literature indicates that the diameter of PVDF electrospun fibers gradually decreases with increasing applied voltage,[21] yet the relationship between fiber diameter and piezoelectric properties after adding AgNPs requires further validation. Additionally, we observed AgNPs extracted from the silver-containing fiber dressing leachate, which were fixed with electron microscopy fixative and analyzed using transmission electron microscopy/energy dispersive spectroscopy (TEM-EDS). The results revealed that some silver nanoparticles were aggregated while others remained dispersed, with aggregated particle sizes ranging from 9 to 24 nm in diameter (Figure 1Bviii, Figure 1C and Figure S2b).

Good piezoelectric performance is a critical prerequisite for the therapeutic efficacy of these self-powered fiber dressings. Based on morphological results, we can discuss the relationship between diameter, AgNPs/PVDF ratio, and piezoelectric performance. From Figure 2A, we obtained characteristic spectral bands for the three crystalline phases of six samples with different silver contents from the ATR-FTIR spectra showing specific vibrational states. The band at 840 cm-1 is designated as the characteristic band of the β phase.[25–28] According to an established equation,[29] we calculated the β phase fraction (F(β), as shown in Table 2). For 12 wt% PVDF at a flow rate of 0.6 mL/h, the relative intensities of peaks corresponding to the α and γ phases decreased with the addition of AgNPs, while the proportion of the β phase increased with the silver content. Thus, we conclude that the addition of silver can promote the formation of the β phase. According to Figure 2B, the characteristic peak of the six groups from the XRD patterns were obtained, where the silver-containing materials exhibited almost identical XRD profiles. The strongest and unique peak was located at $2\theta = 20.80$, suggesting similar phase content in the five silver-containing samples. The α phase has no characteristic peak at 18.3, indicating that its proportion in the system is small. Compared to the typical non-polar XRD pattern of pure PVDF, the diffraction patterns of silver-containing samples resemble the polar β phase. Thus, adding silver to electrospun PVDF-based materials promoted the formation of the electrically active β phase, and the disappearance of the peak at

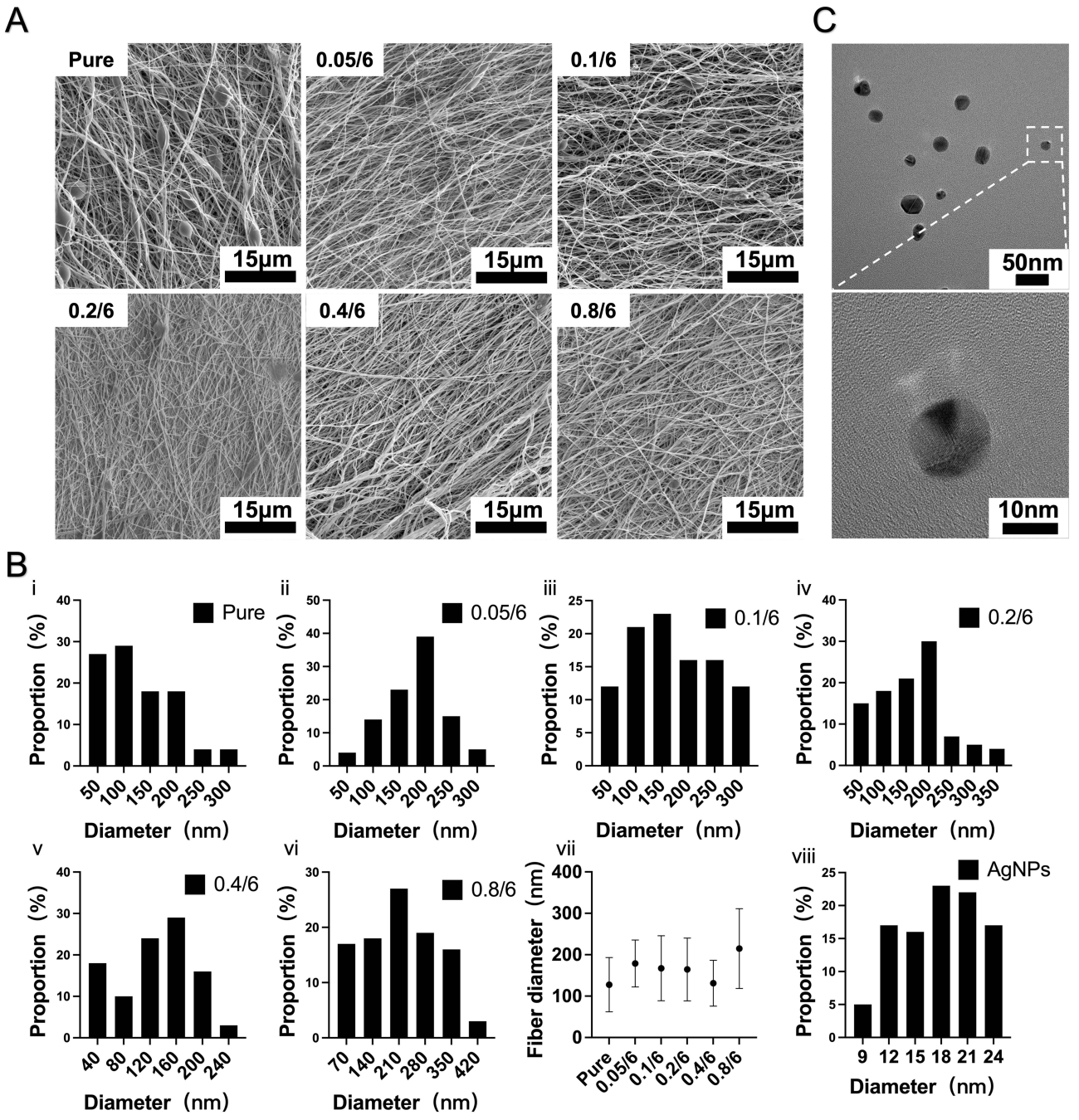

Figure 1 SEM and diameter statistics of each group of fiber dressings and precipitated silver nanoparticles. (**A**) SEM images of Pure (pure PVDF film), 0.05/6, 0.1/6, 0.2/6, 0.4/6, and 0.8/6. (**B**) Quantitative analysis of fiber spinning diameters for each group (i–viii) and quantitative analysis of precipitated silver nanoparticle sizes (h). (**C**) SEM image of precipitated silver nanoparticles.

18.3 facilitated the transition from α to β phase, which enhanced the piezoelectric effect. The DSC thermal analysis (Figure 2C) showed similar curves for all groups, indicating that adding silver had no influence on peak shifts. The butterfly-shaped hysteresis-voltage curves for all materials were shown in Figure 2D, whose amplitudes were varied with the voltage, indicating the existence of piezoelectric effect. Silver-containing PVDF exhibited a more symmetrical shape and size around the crossing points, attributed to enhanced electrical conductivity that dissipated the built-in electric field.

These curves showed small amplitudes and weak piezoelectricity when the silver content is below 0.2/6, while those above 0.2/6 became more symmetrical, confirming that increased silver content leads to aggregation. That aligned with

https://doi.org/10.2147/IJN.S506489

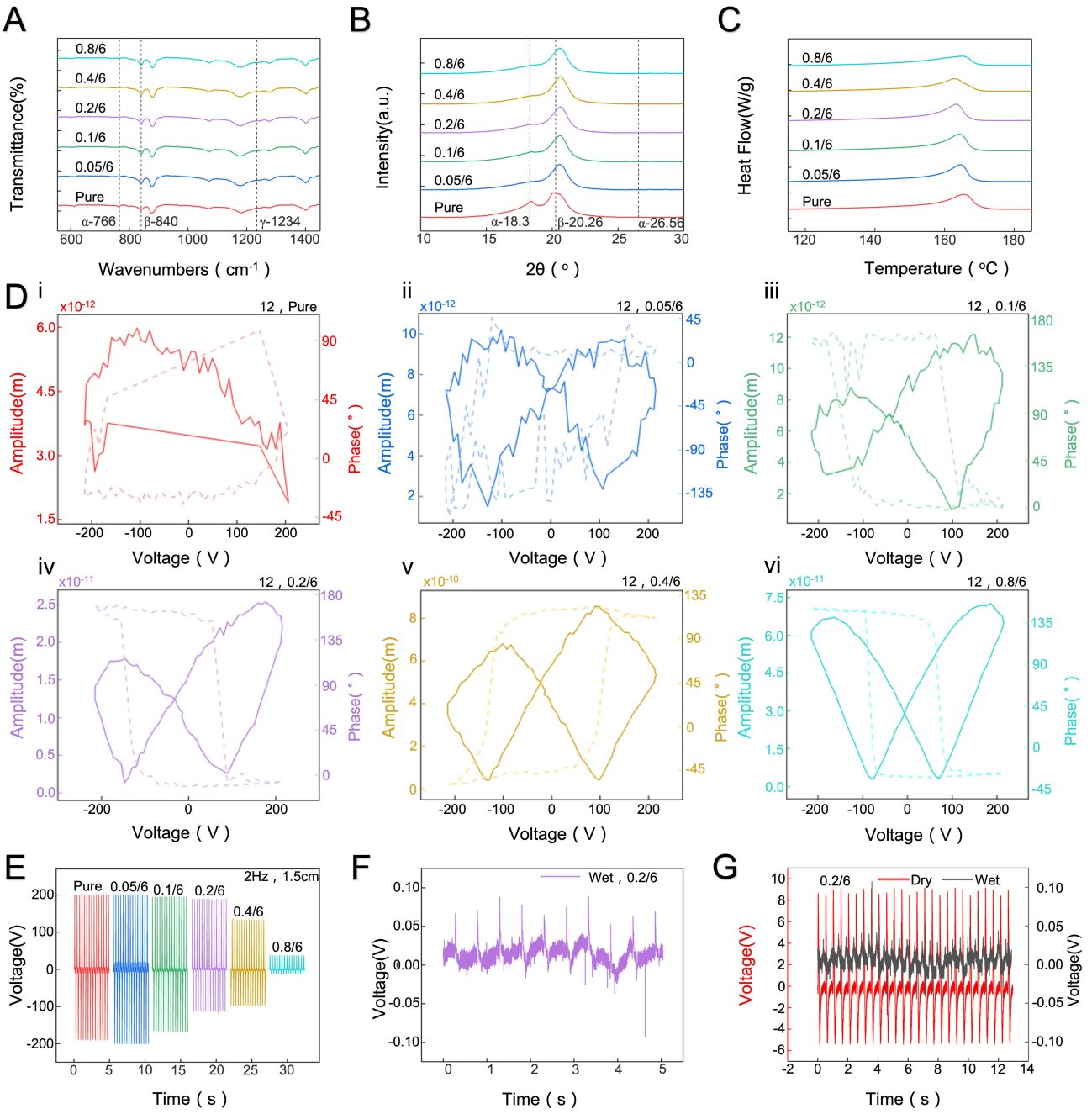

Figure 2 Phase structure characterization and piezoelectric effect of each group of fiber dressings. (**A**) ATR-FTIR results for Pure (pure PVDF film), 0.05/6, 0.1/6, 0.2/6, 0.4/6, and 0.8/6. (**B**) XRD characterization results for each group of fiber dressings. (**C**) DSC characterization results for each group of fiber dressings. (**D**) PFM verification of the piezoelectric effect of each group (i–vi) of fiber dressings. (**E**) Output performance of electrical signals from each group of fiber dressings. (**F** and **G**) Output voltage performance of fiber dressings wetted in PBS solution at pH 6.06.

the trend of β phase fraction and enhanced piezoelectricity. Bending tests further validated the impact of AgNPs content, the maximum output voltage ranked from highest to lowest as follows (Figure 2E): Pure > 0.05/6 > 0.1/6 > 0.2/6 > 0.4/6 > 0.8/6. This is due to an increase in the electrical conductivity of the silver nanoparticles resulting in a decrease in output (Vmax values: Pure: 201.3; 0.05/6: 201.0; 0.1/6: 197.0; 0.2/6: 191.5; 0.4/6: 134.7; 0.8/6: 37.4).[23] When the AgNPs/PVDF ratio was 0.4/6 and 0.8/6, excessive silver leads to significant leakage current.

Then, considering that the materials may encounter moist conditions, such as exudates. The corresponding exudate tests was thus carried out to simulate potential challenges. A PBS solution was used at pH 6.06 to wet the materials, followed by

Table 2 Fractions of β Phase, Melting Enthalpy, Melting Point, and Crystallinity for Each Group

Group	F(β) (%)	Melting Enthalpy (J/g)	Melting Point (°C)	Crystallinity (%)
Pure	70.7	52.1	155.3	51.9
0.05/6	80.4	48.8	156.3	48.1
0.1/6	81.0	47.6	155.7	46.9
0.2/6	86.4	44.9	155.3	44.0
0.4/6	87.1	42.7	153.3	41.8
0.8/6	87.4	38.6	146.9	37.8

conducting voltage testing. For the 0.2/6 group, the output voltage significantly decreased after wetting, showing reduced stability compared to the dry film. The same parameters measured post-wetting indicated a voltage drop, due to the PBS solution restricting the deformation and piezoelectric response of the PVDF fibers (Figures 2F and 2G). Nevertheless, the achievable piezoelectric strength remains sufficient to promote cell migration for wound healing.[30,31]

In vitro Experiments

The electrospun fiber mats exhibit suitable flexibility, excellent electrical performance, and lightweight texture. Before using them as materials to promote wound healing, their antibacterial properties and biocompatibility were further explored.

The antibacterial action and efficacy depend on the nanoparticle size, the PVDF/AgNPs mass ratio, and the spinning process. To select the most suitable material, the antibacterial characteristics of each group against *E. coli* and *S. aureus* were further investigated. As shown in Figures 3A and 3B, OD value decreased and bacterial concentration decreased with the increase of silver content, indicating better antibacterial effect. The pure, 0.05/6, and 0.1/6 groups demonstrated poor antibacterial performance and were excluded. Figures 3C and 3D exhibited the effects of the materials on *S. aureus* and *E. coli*, respectively. Compared with the control group, nanoparticles silver obviously facilitated the disruption of bacterial biofilms; when bacteria contacted the material, silver nanoparticles tended to aggregate and disrupt the biofilm structure.[32] The antibacterial effect was more pronounced against to *S. aureus*, which may be attributed to the structural differences between Gram-positive and Gram-negative bacteria.[33]

The cumulative release method with equal volume was used to observe the silver ion release capability. The maximum release capacity of nanoparticles silver in the materials was simulated by quantitatively taking out the leachate at observation points and adding PBS to maintain a constant volume. Clinically, fiber dressings are primarily used on damaged wounds, where local wound exudate generally only wets the material. Therefore, this cumulative release test was selected to evaluate the total amount of silver nanoparticles released under extreme conditions. As previously mentioned, the mass ratio of the two materials used in the PVDF-AgNPs fiber dressing affects the fiber performance, structural characterization, and piezoelectric properties, thus resulting in differences in silver nanoparticle release capability. The cumulative release curves derived from leachates of different groups were analyzed using iCAP7600 (Figure 3E), showing significant variations in silver release rates among different mass ratios. The 0.05/6, 0.1/6, and 0.2/6 groups exhibited stable silver release with no significant detachment from the fiber dressings, while the 0.4/6 and 0.8/6 groups showed significantly higher releases, especially 0.8/6. This confirms our earlier findings that the high silver content in the 0.4/6 and 0.8/6 groups leads to instability and current leakage. Additionally, while a rapid release rate is beneficial for early-stage antibacterial effects, it is detrimental to wound healing and increases the risk of residual nanoparticles entering the body.

Based on prior stability tests for evaluations of antibacterial capabilities and silver ions, the 0.2/6 mass ratio material was ultimately selected as the representative for further studies in the PVDF-AgNPs group (Figure S3 and Figure S4a, b). To assess the material's impact on cell proliferation, Human Dermal Fibroblasts (HDF) were seeded in 96-well plates and treated with leachate from each group for 4, 16, and 24 hours. Cell viability was measured using the CCK-8 kit. The

 https://doi.org/10.2147/IJN.S506489

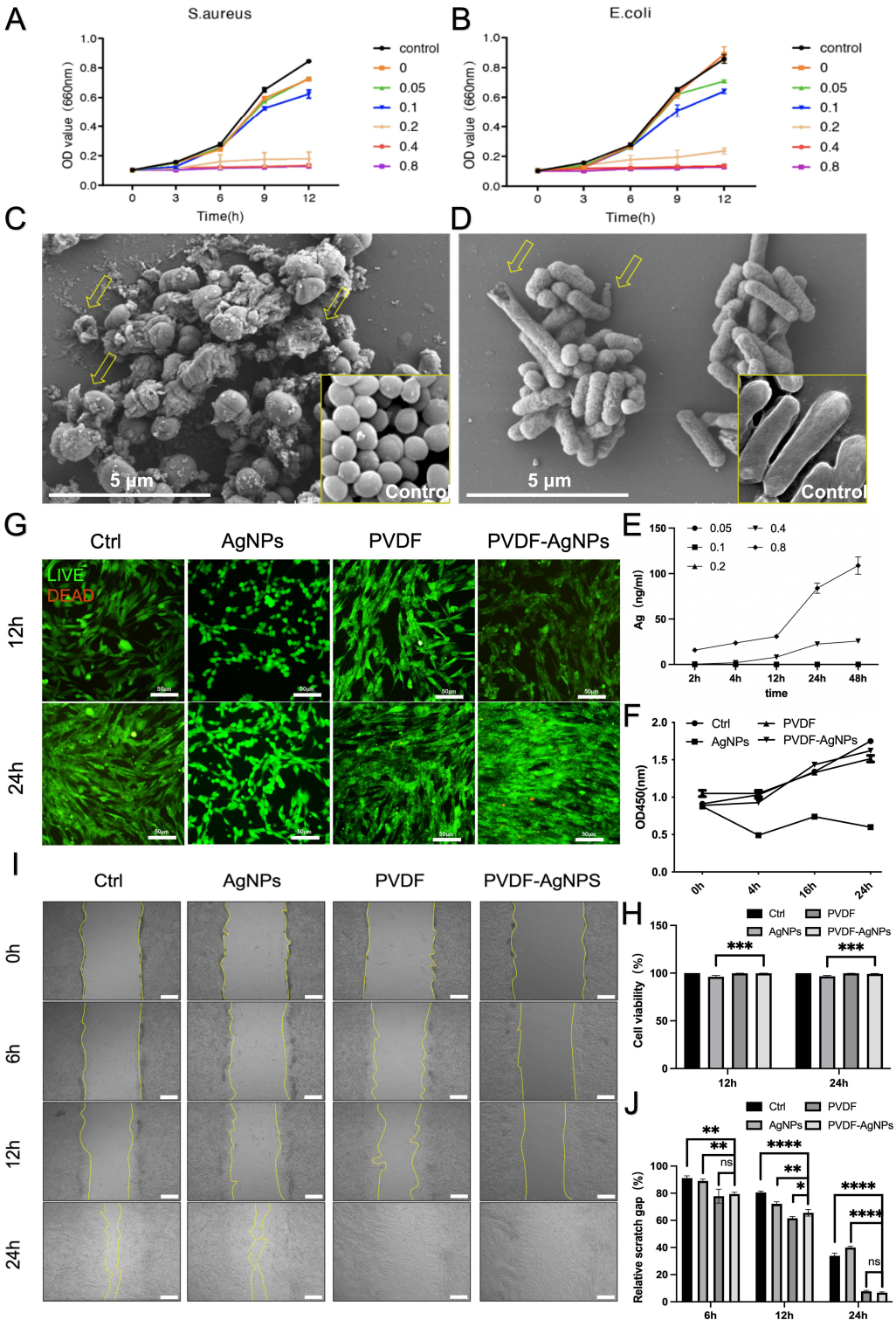

Figure 3 In Vitro Experiments of Electrospun Fiber Dressings. (**A** and **B**) The antibacterial effects of the fiber dressings against *S. aureus* and *E. coli* were explored through the OD values of the leachate from the materials. (**C** and **D**) SEM images of *S. aureus* and *E. coli* after exposure to the fiber dressings (yellow arrows indicate areas of bacterial biofilm disruption). (**E**) Nanoparticle silver release curves for Pure (pure PVDF membrane), 0.05/6, 0.1/6, 0.2/6, 0.4/6, and 0.8/6 groups. (**F**) CCK-8 cytotoxicity assay for the control group, AgNPs, PVDF, and materials group (using 0.2/6 as an example). (**G** and **H**) Live & Dead staining tests for Human Dermal Fibroblasts (HDF) cultured in leachate from the control group, AgNPs, PVDF, and materials group (using 0.2/6 as an example) for 12 and 24 hours, scale bar = 50 μm, and quantification of HDF cell migration at 0, 6, 12, and 24 hours. (**I** and **J**) Migration assays for HDF in leachate environments from the control group, AgNPs, PVDF, and materials group (using 0.2/6 as an example) at 0, 6, 12, and 24 hours, observed under a 4x microscope, along with quantification of HDF cell migration at those time points scale bar = 500 μm.
Notes: Data are presented as mean ± SD (n = 3), *P < 0.05, ** P < 0.01, ***P < 0.005, ****P < 0.001.
Abbreviation: ns, not significant.

results indicated that the control group, PVDF, and PVDF-AgNPs (0.2/6 group as an example) had minimal effects on cell proliferation, while the AgNPs group exhibited significant inhibitory effects on cell viability (Figure 3F). To further confirm material toxicity and evaluate cell proliferation, Figure 3G showed that the control group exhibited many live cells with almost no dead cells. The PVDF and PVDF-AgNPs groups exhibited abundant overlapping live cells and a few red-stained dead cells. In contrast, the AgNPs group displayed a significantly lower density of live cells, and cell proliferation activity was lower than that of the other three groups (Figure 3H). These results indicated that high concentrations of AgNPs can damage cells and inhibit cell growth (Figure S4c), which was consistent with the CCK-8 assessment. Cell migration capability is crucial in wound remodeling and mediating wound regeneration.[34] The effect of the fiber dressings on fibroblast migration was evaluated through scratch assays. As observed in Figures 3I and 3J, both the PVDF and PVDF-AgNPs groups nearly completely healed within 24 hours, with no statistical difference between the two groups. Moreover, there have less remaining area compared to the control and AgNPs groups. This can be attributed to the electrospun fiber dressings effectively releasing conductive elements from the culture medium in the plates to the cells, promoting their migration.

In vivo Experiment

Before the in vivo experiment, the tensile strength of PVDF-AgNPs and PVDF dressings was been investigated. As shown in Figure S5, the tensile strength of PVDF is 54.2 MPa, whereas that of PVDF-AgNPs is slightly higher at 66.7 MPa. Additionally, the elongation at break for PVDF is 151.4%, while PVDF-AgNPs exhibit a slightly lower elongation at break of 148.5%. To determine whether the PVDF-AgNPs piezoelectric antibacterial nanofiber dressing affects wound healing, an infectious wound rat model was constructed. The rats were randomly divided into four groups (Figure 4A), and a 2 cm full-thickness skin defect was created on their backs (Figure 4B), followed by the application of a *S. aureus* suspension. On days 0, 3, 6, 9, and 12, the wounds were covered with gauze (Ctrl group), gauze with AgNPs solution (AgNPs group), PVDF film, or PVDF-AgNPs dressing. Meanwhile, the images were recorded, and samples were taken.

On day 12, the wound healing area percentages for the Ctrl group, AgNPs group, PVDF group, and PVDF-AgNPs group were 39.44 ± 12.74%, 67.09 ± 9.99%, 69.52 ± 6.26%, and 93.57 ± 5.07% (Figure 4C and 4D), respectively. The wounds in the rats treated with PVDF-AgNPs dressings (Figure S6a) were closed significantly faster, and the wounds appeared elongated. Moreover, purulent exudate, local redness, swelling, and other inflammatory symptoms were relatively mild (Figure S6b). This is because the movement of the rat's back primarily involves vertical bending in the direction parallel to the spine, leading to a unidirectional electric field that promotes the directional migration of cells and signaling molecules due to electrotaxis.[35] Electrical stimulation also contributed to wound contraction (Figure 4E), causing a narrowing of the overall wound width (Figure 4F and 4G). This suggested that we can intervene in the direction of the electric current to relieve tension in areas with high local tension. Furthermore, the other groups exhibited significantly slower wound healing rate.

Histological evaluation further revealed the therapeutic effect of the self-powered fiber membrane by elucidating the healing process of regenerating tissues. Histological analysis on skin sections from each group of rats were performed using HE staining Masson staining, and CD68 immunofluorescence staining to obtain more detailed insights related to skin regeneration. As the largest functional structure in the human body, the performance of blood vessels, collagen, and inflammatory cells is typically used to assess the maturity of tissue regeneration and the newly formed skin structure.[36,37]

As shown in Figure 5Ai, the formation of new blood vessels in all groups were observed. The PVDF and PVDF-AgNPs groups exhibited significant epithelial crawling, high coverage, thicker tissue, and a curved epithelial migration path. In the later stages, more distinct fibrous structures and angiogenesis were showed. Additionally, collagen fibers are another indicator of the maturity of the newly formed skin. According to Figure 5Aii, collagen deposition increased over time in all groups. On day 12, the collagen deposition in the blue-stained areas of the materials containing PVDF was noticeably thicker compared to the other groups, with the PVDF-AgNPs group showing interlaced, blue-stained collagen and red-stained fibrous structures, primarily located in the upper dermis near the material.

Macrophages, essential immune cells, play a key role in immune responses due to their plasticity and function as either pro-inflammatory or anti-inflammatory agents. Macrophage infiltration and activation are often involved in wound healing.[38] Using CD68 immunofluorescence staining, a classic macrophage marker, we found that inflammatory

 https://doi.org/10.2147/IJN.S506489

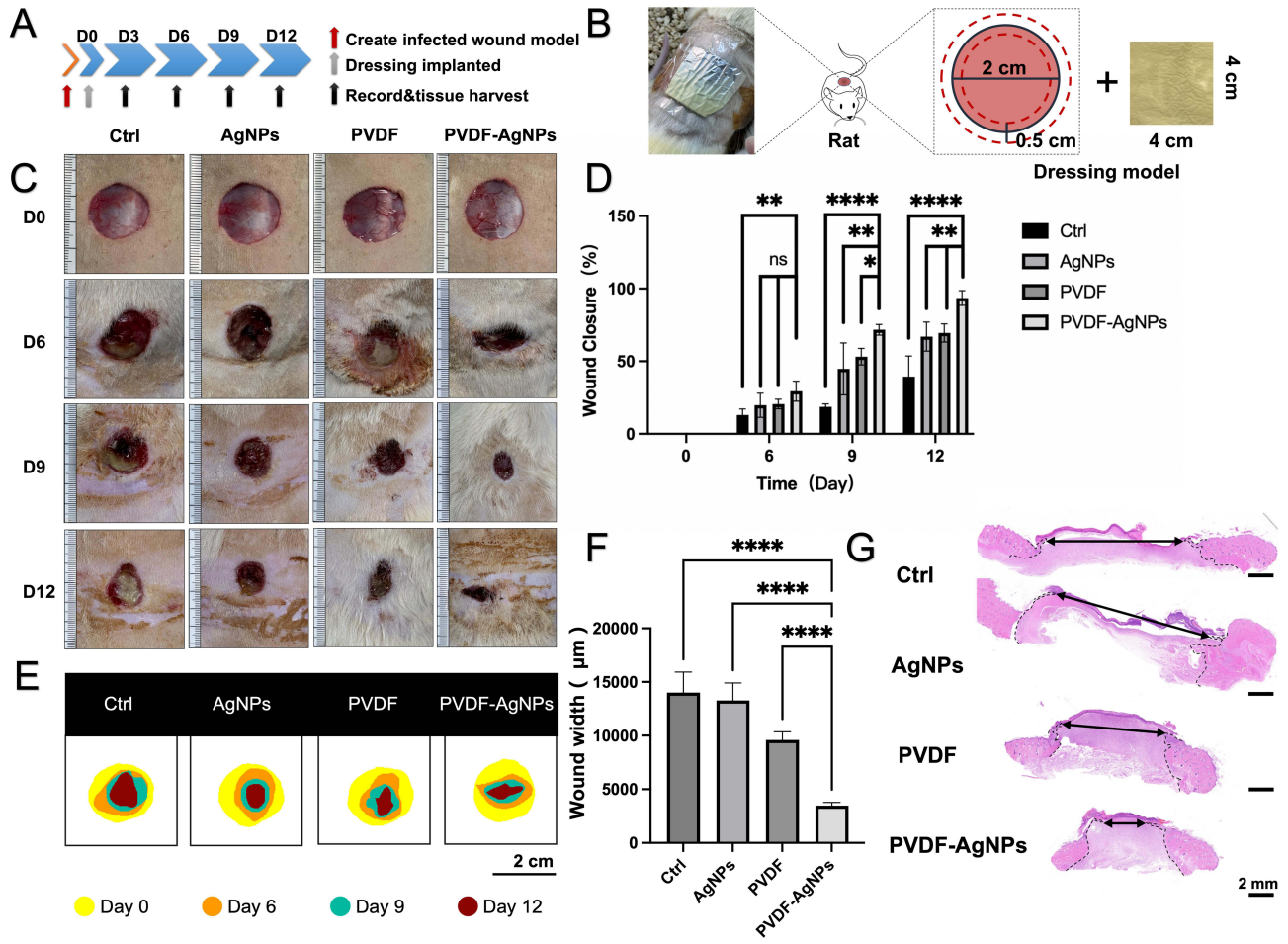

Figure 4 The effect of PVDF-AgNPs on infected wound healing and re-epithelialization. (**A** and **B**) Schematic of the establishment of the *S. aureus* infection wound model, with observations and sampling conducted on days 0, 3, 6, 9, and 12. (**C**) Representative images of rat wounds on days 0, 6, 9, and 12 following treatments with gauze (Ctrl group), gauze containing AgNPs solution (AgNPs group), PVDF membrane, and PVDF-AgNPs membrane. (**D**) Quantitative analysis of wound healing rates on days 0, 6, 9, and 12. (**E**) Analysis of wound healing traces on days 0, 6, 9, and 12. (**F**) Quantitative analysis of HE-stained section widths on day 12 for each group. (**G**) HE-stained section images of wounds from each group on day 12. Scale bar: 2 mm. The black arrow indicates the width of the wound.
Notes: Data are presented as mean ± SD (n = 5), *P < 0.05, **P < 0.01, ****P < 0.001.
Abbreviation: ns, not significant.

infiltration was most severe on days 6 and 9, with widespread fluorescence staining. The two groups containing AgNPs exhibited less inflammatory cell infiltration and milder inflammation (Figure 5Aiii).

The immune microenvironment in wounds plays a crucial role in preventing pathogen invasion and tissue regeneration. Under the stimulation of interferon-γ (IFN-γ) and tumor necrosis factor-α (TNF-α), M1 macrophages dominate the early stages of wound healing, producing pro-inflammatory mediators such as interleukin-6 (IL-6) to promote the initial inflammatory response. In contrast, M2 macrophages secrete interleukin-10 (IL-10) through polarization, which reduces inflammation, promotes collagen deposition and enhances tissue repair.[39–43] Quantitative analysis of inflammatory factors in the skin of each group of rats via enzyme-linked immunosorbent assay (ELISA) revealed that the levels of pro-inflammatory factors TNF-α and IL-6 in the PVDF-AgNPs group (315.13 ± 75.97 pg/mL and 179.78 ± 41.01 pg/mL, respectively) were significantly lower than those in the PVDF group (1414.54 ± 142.16 pg/mL and 336.84 ± 52.29 pg/mL, respectively) (Figure 5B). Additionally, the anti-inflammatory factor IL-10 secreted by M2 macrophages was higher in the PVDF-AgNPs group (371.00 ± 32.37 pg/mL) compared to the Ctrl and PVDF groups (225.71 ± 25.49 pg/mL), indicating that the addition of AgNPs effectively enhanced the anti-inflammatory capability of the material. Although the IFN-γ level in the PVDF-AgNPs group (103.47 ± 13.89 pg/mL) was lower than in the Ctrl group (145.82 ± 12.27 pg/mL) (Figure S6c), there was no significant difference between the PVDF-AgNPs (124.41 ± 15.29 pg/mL) and PVDF groups.

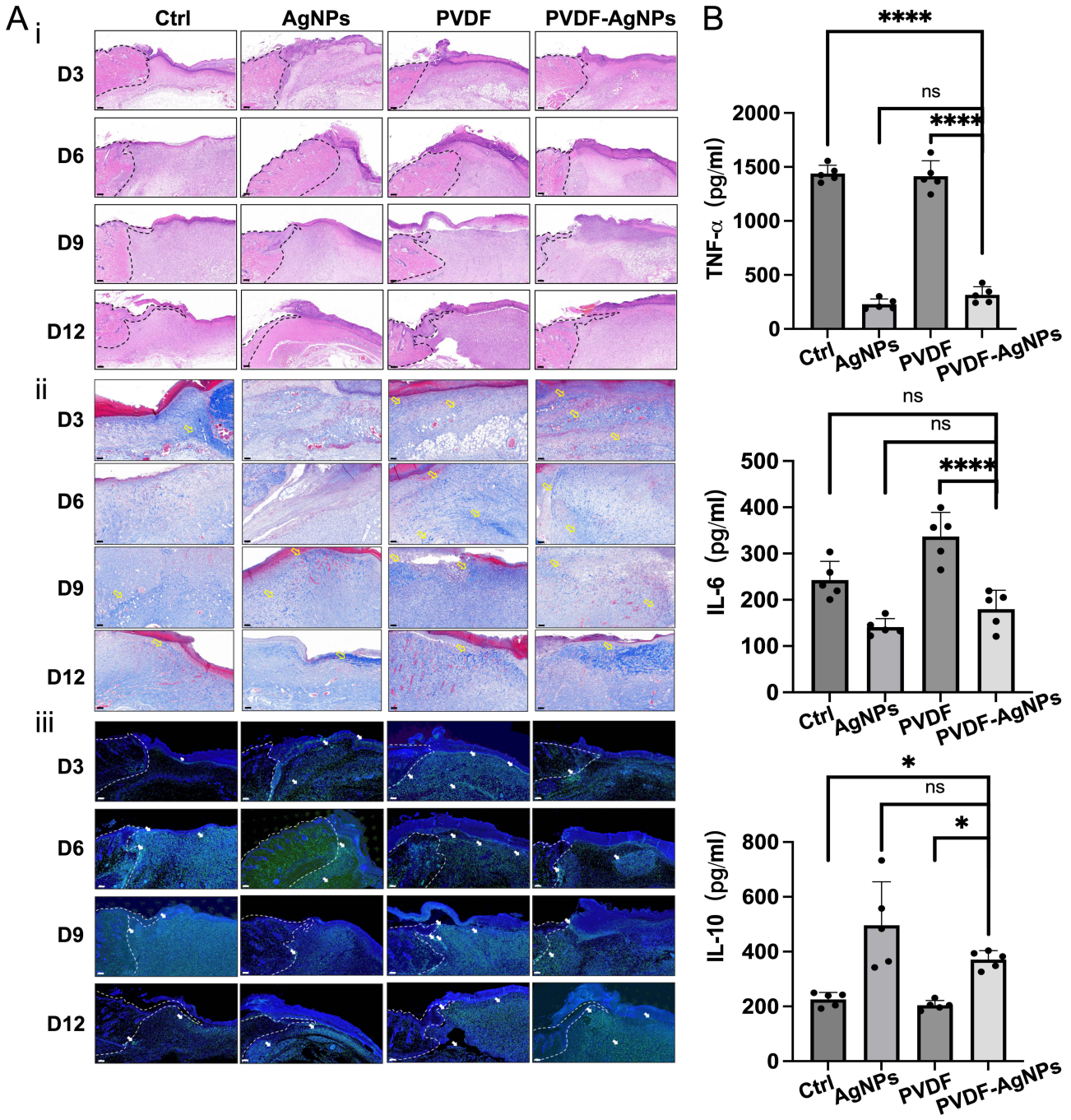

Figure 5 Histological presentation of wound healing on days 3, 6, 9, and 12. (**A**) i: HE-stained images of the newly formed skin tissue, scale bar 200 μm; ii: Masson-stained images of the newly formed skin tissue, scale bar 100 μm; iii: CD68 immunofluorescence-stained images of the newly formed skin tissue, scale bar 200 μm. (**B**) Quantitative analysis of the expression levels of TNF-α, IL-6, and IL-10 on day 12 of wound healing.
Notes: Data are presented as mean ± SD (n = 5), *P < 0.05, ****P < 0.001.
Abbreviation: ns, not significant.

This may be attributed to the intrinsic ability of the piezoelectric material to enhance the local immune response and regulate IFN-γ levels.[44]

In chronic wounds, where the conversion from pro-inflammatory to anti-inflammatory macrophages and tissue repair is impaired, inducing macrophages with beneficial phenotypes is crucial for wound treatment.[38,45,46] The classic M1 marker (CD86) and M2 marker was used (CD206) for immunofluorescence co-staining.[39] As shown in Figure 6A and 6B, the total number of macrophages on days 3, 6, and 12 in the PVDF-AgNPs groups was (11.56 ± 1.22%, 7.52 ± 2.29%

https://doi.org/10.2147/IJN.S506489

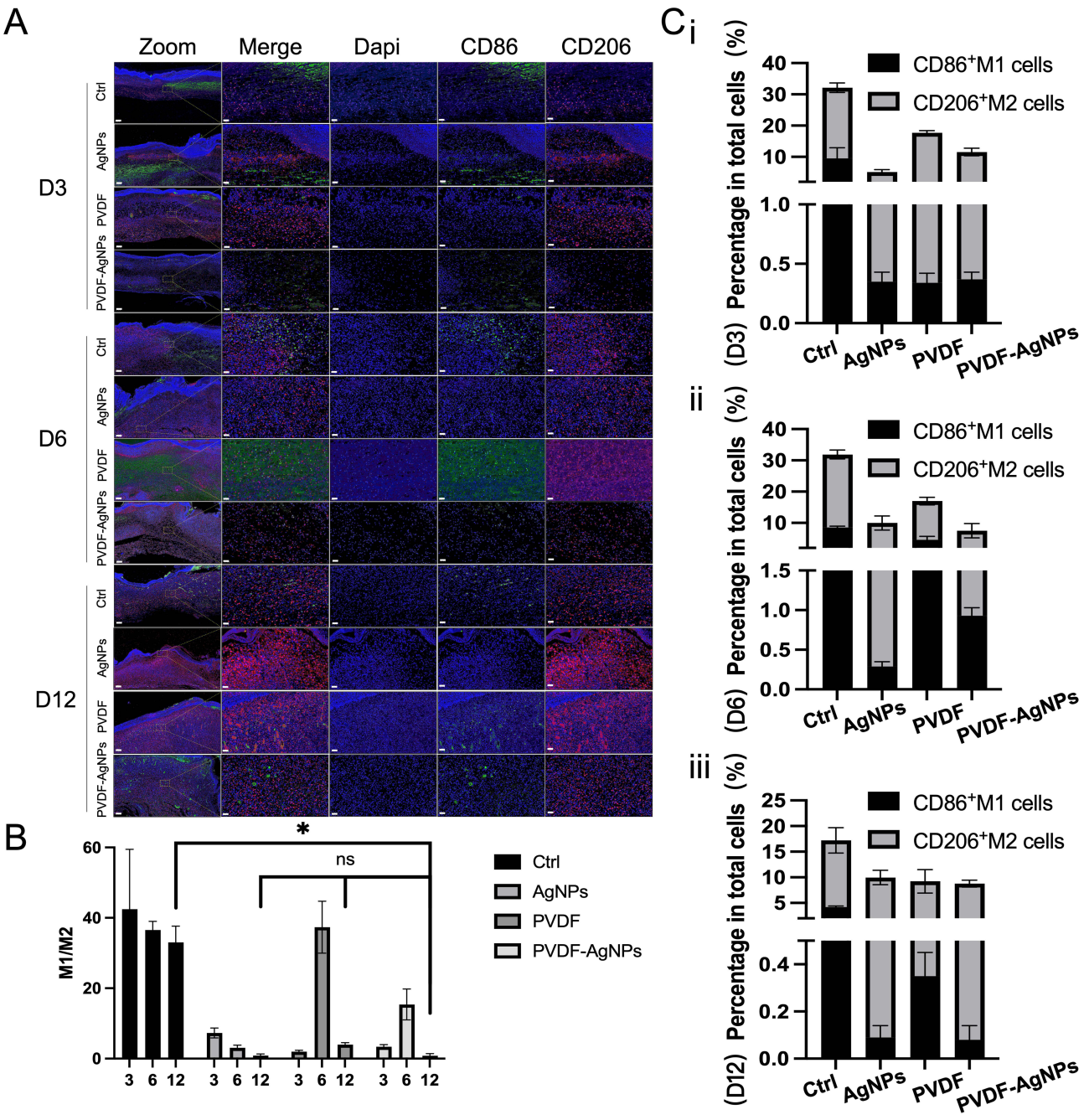

Figure 6 Immunofluorescence staining analysis of M1 and M2 macrophages on days 3, 6, and 12. (**A**) Immunofluorescence staining of wound tissue sections from each group at different time points. CD86 was used as a representative marker for M1 macrophages, and CD206 was used as a representative marker for M2 macrophages. Scale bar: 200 μm. (**B**) Quantitative analysis of the M1/M2 macrophage ratio in each group on days 3, 6, and 12. (**C**) Quantitative analysis of the total number of inflammatory cells and the proportion of M1 and M2 macrophages in each group on days 3, 6, and 12 (i–iii).
Notes: Data are presented as mean ± SD (n = 5), *P < 0.05.
Abbreviation: ns, not significant.

and 8.77 ± 0.68%, respectively) lower to the control group (32.13 ± 3.75%, 31.88 ± 1.46% and 17.22 ± 2.48%, respectively). Furthermore, it could be observed that the proportion of M1 macrophages in the PVDF-AgNPs groups was lower than that in the Ctrl and PVDF groups on day 6 (0.93 ± 0.10%, 8.52 ± 0.42% and 4.61 ± 1.07%, respectively) (Figure 6C). On day 12, the M1/M2 ratio in the PVDF-AgNPs (0.85 ± 0.57), PVDF (4.00 ± 0.55), and AgNPs groups (0.88 ± 0.43) was lower than in the Ctrl group (33.02 ± 4.65) (Figure 6C). This demonstrates that both PVDF and AgNPs, as well as their mixed electrospun material in the PVDF-AgNPs Nanofiber dressing, can reduce the

inflammatory response by modulating macrophage activation.[47,48] Ultimately, PVDF-AgNPs can accelerate the wound healing process in the rat model through their combined effects.

The results indicate that the PVDF-AgNPs self-powered Nanofiber dressing, as a treatment dressing for infected wounds, can continuously achieve good immunomodulatory effects after injury. It reduces the proportion of M1 macrophages in newly regenerated skin tissue, modulates the M1/M2 macrophage ratio within the microenvironment, and activates M2 macrophages, thereby facilitating fibroblast migration, enhancing collagen secretion, and promoting the healing of infected wounds.

Discussion

The electrospinning process and the addition of AgNPs significantly impacted the morphology and properties of the PVDF nanofiber dressings. Choosing a 12 wt% PVDF concentration and a flow rate of 0.6 mL/h proved effective for generating consistent nanofiber structures.[21] The different Ag/PVDF mass ratios allowed us to explore how silver content influences fiber conductivity, biocompatibility, and antibacterial performance, demonstrating the importance of optimizing these parameters for desirable dressing properties.

SEM analysis revealed that pure PVDF fibers exhibited lower conductivity, leading to uneven spinning and bead formation, whereas silver-containing fibers showed a more uniform morphology with fewer beads. This suggests that the inclusion of AgNPs improves the electrospinning process by enhancing conductivity, resulting in more consistent fiber structures. The similar diameter distribution across different Ag/PVDF ratios indicates that silver content does not directly influence fiber diameter, although it impacts uniformity and structure.The ATR-FTIR and XRD analyses confirmed the formation of the electrically active β phase with increased AgNP content, aligning with existing studies indicating that the β phase contributes to enhanced piezoelectric properties in PVDF materials.[25] The addition of AgNPs appeared to facilitate the transition from the α to β phase, which is essential for achieving good piezoelectric performance. This transition is particularly relevant for self-powered dressing applications, as the β phase is known to enhance the piezoelectric effect, potentially contributing to improved therapeutic outcomes in wound healing. Piezoelectric measurements showed that Ag/PVDF ratios above 0.2/6 led to higher electrical conductivity, which in turn decreased the piezoelectric output due to current leakage. This indicates an optimal AgNP content, as excessive silver negatively affects piezoelectric efficiency. Bending tests further supported this, with the 0.2/6 group displaying sufficient output for cell migration, a critical factor for wound healing. The drop in piezoelectric output under moist conditions (PBS solution) suggests that while AgNP-enhanced PVDF fibers are stable in dry environments, their performance may be challenged in wet conditions. However, even with this decrease, the piezoelectric output remained adequate to promote cellular activity, which is beneficial for wound healing applications.[14] The crystallinity and β phase fraction data further reinforce that the addition of AgNPs enhances the piezoelectric properties by promoting β phase formation. However, as shown in the DSC and piezoelectric testing, higher AgNP content (0.4/6 and 0.8/6) leads to a decrease in stability, which is possibly due to the aggregation of silver particles that interferes with the material's structural integrity. The findings suggest that while silver content enhances piezoelectric and antibacterial properties, it requires careful balance to avoid compromising the mechanical and electrical stability of the dressing.

The results indicate that the optimal Ag/PVDF ratio lies around 0.2/6, balancing conductivity, piezoelectric output, and stability in moist environments. Future studies could explore ways to improve the moisture resistance of these dressings while maintaining the therapeutic benefits of piezoelectric stimulation and antibacterial efficacy, furthering their potential for clinical wound care applications.

The in vitro experiments confirmed that PVDF-AgNPs fiber mats exhibit promising antibacterial and biocompatibility properties, making them suitable candidates for wound healing applications. The flexibility, electrical performance, and lightweight nature of these electrospun fibers are advantageous traits that align with the requirements for effective wound dressings.

The antibacterial efficacy of the PVDF-AgNPs fibers was influenced by the silver nanoparticle size, PVDF/AgNPs mass ratio, and spinning process parameters. The observed reduction in OD values and bacterial concentrations with increased silver content indicates that higher AgNPs content enhances antibacterial effectiveness, particularly against *S. aureus*. The more pronounced antibacterial effect on *S. aureus* compared to *E. coli* can be attributed to structural differences between Gram-positive and Gram-negative bacteria, as Gram-positive bacteria like *S. aureus* are generally

more susceptible to silver due to their thicker peptidoglycan layer, which facilitates silver ion penetration.[9,15] The cumulative release study highlighted the impact of silver content on the stability and release characteristics of the dressings. While groups with lower silver content (0.05/6, 0.1/6, and 0.2/6) exhibited stable and controlled silver release, higher silver concentrations (0.4/6 and 0.8/6) led to significant increases in release rates, potentially compromising dressing stability. Although a rapid initial release of silver can be beneficial for early-stage antibacterial action, excessive release may inhibit wound healing and increase the risk of nanoparticle accumulation within the body. These findings align with the previous observations of instability and current leakage in the higher silver content groups, further suggesting that a balanced Ag/PVDF ratio is critical for optimizing dressing performance.The biocompatibility assessments indicated that the PVDF-AgNPs (0.2/6) group had minimal cytotoxic effects on Human Dermal Fibroblasts (HDFs), as evidenced by both the CCK-8 assays and live/dead staining results. In contrast, high concentrations of AgNPs significantly inhibited cell viability, indicating that while silver is beneficial in controlled amounts, excessive exposure can be cytotoxic. These results suggest that the 0.2/6 PVDF-AgNPs ratio offers an optimal balance, providing antibacterial benefits without compromising cell viability.The scratch assays demonstrated that the PVDF-AgNPs dressing effectively promotes fibroblast migration, which is crucial for wound healing. The ability of these dressings to facilitate near-complete wound closure within 24 hours highlights their potential role in wound remodeling and regeneration. The conductive properties of the PVDF-AgNPs dressing likely contribute to this effect by enhancing cellular migration, thus aiding in the healing process.

In summary, the in vitro findings support the selection of the 0.2/6 PVDF-AgNPs ratio as an optimal formulation for wound dressing applications. This composition offers a favorable balance of antibacterial efficacy, controlled silver release, and biocompatibility, making it a promising candidate for further in vivo evaluation in wound care settings.

The in vivo experiments using an infected wound model in rats demonstrated that PVDF-AgNPs piezoelectric antibacterial nanofiber dressings significantly promote wound healing by modulating both wound contraction and the immune response. Compared with existing AgNP-loaded dressings,[49] our PVDF-AgNP dressing shares the advantages of excellent antibacterial and anti-inflammatory properties. However, our dressing further demonstrates superior performance through its piezoelectric stimulation, which promotes fibroblast migration and tissue regeneration more effectively. In addition, our design optimizes silver release to balance antibacterial efficacy and cytotoxicity, addressing a key limitation of many existing dressings. The PVDF-AgNPs dressing achieved faster wound closure compared to the control and other treatment groups, with marked reduction in inflammatory symptoms such as purulent exudate, redness, and swelling. This rapid wound healing effect can be attributed to the directional electric field generated by the piezoelectric properties of the PVDF-AgNPs, which facilitates the electrotactic migration of cells and signaling molecules, thereby enhancing wound contraction and re-epithelialization.

Histological analysis further corroborated the therapeutic effects of the PVDF-AgNPs dressing by revealing enhanced collagen deposition, angiogenesis, and epithelial migration in the treated wounds. The newly formed skin in the PVDF-AgNPs group showed well-organized fibrous structures and significant collagen accumulation, particularly in the upper dermis, which is crucial for restoring skin integrity. The enhanced collagen deposition and angiogenesis suggest that the PVDF-AgNPs dressing not only supports faster wound closure but also contributes to the maturation and stability of the regenerating tissue.Macrophage modulation was a key factor in the observed healing process. The PVDF-AgNPs dressing demonstrated an ability to regulate macrophage polarization, shifting the balance from pro-inflammatory M1 macrophages to anti-inflammatory M2 macrophages. This shift was evidenced by the lower levels of pro-inflammatory cytokines (TNF-α and IL-6) and higher levels of the anti-inflammatory cytokine IL-10 in the PVDF-AgNPs group. By reducing M1 macrophage activity and promoting M2 macrophage activation, the PVDF-AgNPs dressing creates a favorable immune microenvironment that supports tissue repair and reduces excessive inflammation, which is critical for healing infected wounds.The immunomodulatory effects of the PVDF-AgNPs dressing were further supported by the lower M1/M2 macrophage ratio and reduced overall macrophage infiltration in the treated wounds. The reduction in M1 macrophage markers (CD86) and the increase in M2 markers (CD206) indicate that the PVDF-AgNPs dressing effectively shifts the immune response from a pro-inflammatory to a reparative state, which is essential for chronic wound healing. This immune modulation, combined with the antibacterial properties of AgNPs, enables the PVDF-AgNPs dressing to combat infection while promoting a healing-favorable microenvironment.

The findings emphasize the role of AgNP content in optimizing the piezoelectric, antibacterial, and biocompatibility properties of PVDF-AgNPs dressings. The identified 0.2/6 ratio demonstrates a balance of these attributes, resulting in enhanced cellular responses and wound healing performance. Future studies should further investigate strategies to improve the moisture resistance and mechanical stability of these dressings,[50–53] as well as validate their performance in larger-scale preclinical and clinical models.

Conclusion

In this study, a micro-electro nanofiber dressing based on PVDF-AgNPs using electrospinning technology was successfully developed. By precisely controlling process parameters such as PVDF concentration, Ag/PVDF mass ratio, and solution flow rate, we further optimized the values. These fiber membranes exhibited excellent piezoelectric performance and significant antibacterial effects. The optimized PVDF-AgNPs dressing featured a uniform nanofiber structure and remarkable piezoelectric properties. In vitro and in vivo studies confirmed that these nanofiber dressings possess good biocompatibility, promoting fibroblast migration, collagen deposition, and re-epithelialization, thus significantly accelerating wound healing. The addition of nanosilver further provided antibacterial protection, effectively controlling local wound infections and promoting the healing of infected wounds. However, this study also highlights several challenges and limitations that must be addressed in future research. Firstly, the moisture sensitivity of the piezoelectric properties under wet or highly exudative wound conditions presents a challenge to maintaining the dressing's optimal performance, particularly in wounds with excessive exudates. Secondly, the long-term safety and stability of PVDF-AgNPs nanofiber dressings in clinical applications require further exploration, as prolonged exposure to nanosilver could potentially lead to cytotoxicity or environmental concerns. This PVDF-AgNPs Nanofiber dressing could serve as a personalized "energy skin" for wound applications, addressing both infection control and wound healing, opening up its potential for clinical applications in modern wound care. Future studies should focus on improving the mechanical and moisture resistance properties of these dressings while ensuring their long-term safety and therapeutic benefits.

Acknowledgments

The authors gratefully acknowledge the financial Supported by Biomaterials and Regenerative Medicine Institute Cooperative Research Project, Shanghai Jiaotong University School of Medicine (project number 2022LHA05); the Interdisciplinary Program of Shanghai Jiao Tong University (project number YG2019QNA15); Shanghai Clinical Research Center of Plastic and Reconstructive Surgery supported by Science and Technology Commission of Shanghai Municipality (project number 22MC1940300); Wang Zhengguo Foundation for Traumatic Medicine Growth Factor Rejuvenation Plan (project number SZYZ-TR-13); Basic Research Promotion Programme supported by The Ninth People's Hospital of Shanghai Jiaotong University School of Medicine (project number JYZZ220).

Author Contributions

T. Liu and F.Xie. contributed equally to this work. All authors made significant contributions to the work, including the conception, study design, execution, data collection, data analysis, and interpretation. All authors were involved in drafting, revising, or critically reviewing the manuscript and gave final approval of the version to be published. They all agree to be accountable for all aspects of the work.

Disclosure

The authors report no conflicts of interest in this work.

References

1. Dorf E, Blue C, Smith BP, Koman LA. Therapy after injury to the hand. *J Am Acad Orthop Surg*. 2010;18(8):464–473. doi:10.5435/00124635-201008000-00003
2. Buckthorpe M, Gokeler A, Herrington L, et al. Optimising the Early-Stage Rehabilitation Process Post-ACL Reconstruction. *Sports Med*. 2024;54(1):49–72. doi:10.1007/s40279-023-01934-w

3. Tan J, Chen J, Zhou J, et al. Joint contractures in severe burn patients with early rehabilitation intervention in one of the largest burn intensive care unit in China: a descriptive analysis. *Burns Trauma*. 2019;7:17. doi:10.1186/s41038-019-0151-6
4. Hosseini M, Brown J, Khosrotehrani K, Bayat A, Shafiee A. Skin biomechanics: a potential therapeutic intervention target to reduce scarring. *Burns Trauma*. 2022;10:tkac036. doi:10.1093/burnst/tkac036
5. Richard R, Santos-Lozada AR. Burn Patient Acuity Demographics, Scar Contractures, and Rehabilitation Treatment Time Related to Patient Outcomes: the ACT Study. *J Burn Care Res*. 2017;38(4):230–242. doi:10.1097/BCR.0000000000000490
6. Richard R, Santos-Lozada AR, Dewey WS, Chung KK. Profile of Patients Without Burn Scar Contracture Development. *J Burn Care Res*. 2017;38 (1):e62–e69. doi:10.1097/BCR.0000000000000418
7. Dombrecht D, Van Daele U, Van Asbroeck B, et al. Molecular mechanisms of post-burn muscle wasting and the therapeutic potential of physical exercise. *J Cachexia Sarcopenia Muscle*. 2023;14(2):758–770. doi:10.1002/jcsm.13188
8. Chen K, Wu Z, Liu Y, Yuan Y, Liu C. Injectable double-crosslinked adhesive hydrogels with high mechanical resilience and effective energy dissipation for joint wound treatment. *Adv. Funct. Mater.* 2022;32(12):2109687. doi:10.1002/adfm.202109687
9. Ma W, Ling S, Liu Y, Chen Z, Xu J. Bio-inspired low-cost fabrication of stretchable, adhesive, transparent, and multi-functionalized joint wound dressings. *ACS Appl Mater Interfaces*. 2023;15(19):22915–22928. doi:10.1021/acsami.3c02065
10. Hu Q, Du Y, Bai Y, et al. Sprayable Zwitterionic Antibacterial Hydrogel With High Mechanical Resilience and Robust Adhesion for Joint Wound Treatment. *Macromol Rapid Commun*. 2024;45(8):2300683. doi:10.1002/marc.202300683
11. Zhou X, Feng P, Liu H, Song B. Bioinspired aligned wrinkling dressings for monitoring joint motion and promoting joint wound healing. *Biomater Sci*. 2022;10(18):5146–5157. doi:10.1039/D2BM00602B
12. Cai C, Zhu H, Chen Y, et al. Mechanoactive nanocomposite hydrogel to accelerate wound repair in movable parts. *Acs Nano*. 2022;16 (12):20044–20056. doi:10.1021/acsnano.2c07483
13. Ding X, Yu Y, Fan L, et al. Sprayable Multifunctional Black Phosphorus Hydrogel with On-Demand Removability for Joint Skin Wound Healing. *Adv Healthc Mater*. 2024;13(4):e2302588. doi:10.1002/adhm.202302588
14. Chen SK, Liu JJ, Wang X, et al. Hericium erinaceus β-glucan/tannic acid hydrogels based on physical cross-linking and hydrogen bonding strategies for accelerating wound healing. *Int J Biol Macromol*. 2024;279(Pt 4):135381. doi:10.1016/j.ijbiomac.2024.135381
15. Xu J, Fan Z, Duan L, Gao G. A tough, stretchable, and extensively sticky hydrogel driven by milk protein. *Polym Chem*. 2018;2018(19):9.
16. Ojingwa JC, Isseroff RR. Electrical stimulation of wound healing. *J Invest Dermatol*. 2003;121(1):1–12.
17. Luo R, Dai J, Zhang J, Li Z. Accelerated Skin Wound Healing by Electrical Stimulation. *Adv Healthc Mater*. 2021;10(16):e2100557. doi:10.1002/adhm.202100557
18. Bourguignon GJ, Bourguignon LY. Electric stimulation of protein and DNA synthesis in human fibroblasts. *FASEB j*. 1987;1(5):398–402. doi:10.1096/fasebj.1.5.3678699
19. Slabov V, Kopyl S, Dos Santos MP S, Kholkin AL. Natural and Eco-Friendly Materials for Triboelectric Energy Harvesting. *Nanomicro Lett*. 2020;12(1):42. doi:10.1007/s40820-020-0373-y
20. Maity K, Garain S, Henkel K, Schmeißer D, Mandal D. Natural Sugar-Assisted, Chemically Reinforced, Highly Durable Piezoorganic Nanogenerator with Superior Power Density for Self-Powered Wearable Electronics. *ACS Appl Mater Interfaces*. 2018;10(50):44018–44032. doi:10.1021/acsami.8b15320
21. Baqeri M, Abolhasani MM, Mozdianfard MR, Guo Q, Oroumei A, Naebe M. Influence of processing conditions on polymorphic behavior, crystallinity, and morphology of electrospun poly(VInylidene fluoride) nanofibers. *J Appl Polym Sci*. 2015;132(30). doi:10.1002/app.42304
22. Ribeiro C, Sencadas V, Ribelles JLG, Lanceros-Mendez S. Influence of Processing Conditions on Polymorphism and Nanofiber Morphology of Electroactive Poly(vinylidene fluoride) Electrospun Membranes. *Soft Mater*. 2010;8(1–4):274–287. doi:10.1080/1539445X.2010.495630
23. Mandal D, Henkel K, Schmeisser D. Improved performance of a polymer nanogenerator based on silver nanoparticles doped electrospun P (VDF-HFP) nanofibers. *Phys Chem Chem Phys*. 2014;16(22):10403–10407. doi:10.1039/c3cp55238a
24. Kalimuldina G, Turdakyn N, Abay I, et al. A Review of Piezoelectric PVDF Film by Electrospinning and Its Applications. *Sensors*. 2020;20 (18):5214. doi:10.3390/s20185214
25. Shao H, Fang J, Wang H, Lin T. Effect of electrospinning parameters and polymer concentrations on mechanical-to-electrical energy conversion of randomly-oriented electrospun poly(vinylidene fluoride) nanofiber mats. *RSC Adv*. 2015;5(19):14345–14350. doi:10.1039/C4RA16360E
26. Boccaccio T, Bottino A, Capannelli G, Piaggio PJ. Characterization of PVDF Membranes by Vibrational Spectroscopy. *J Membr Sci*. 2002;210 (2):315–329. doi:10.1016/S0376-7388(02)00407-6
27. Salimi A, Yousefi AA. FTIR studies of beta-phase crystal formation in stretched PVDF films. *Polym Test*. 2003;22(6):699–704. doi:10.1016/S0142-9418(03)00003-5
28. Bormashenko Y, Pogreb R, Stanevsky O, Bormashenko E. Vibrational spectrum of PVDF and its interpretation. *Polym Test*. 2004;23(7):791–796. doi:10.1016/j.polymertesting.2004.04.001
29. Gregorio, Jr. R Jr, Cestari M. Effect of crystallization temperature on the crystalline phase content and morphology of poly(vinylidene fluoride). *J Polym Sci B Polym Phys*. 1994;32(5):859–870. doi:10.1002/polb.1994.090320509
30. Nishimura KY, Isseroff RR, Nuccitelli R. Human keratinocytes migrate to the negative pole in direct current electric fields comparable to those measured in mammalian wounds. *J Cell Sci*. 1996;109(Pt 1):199–207. doi:10.1242/jcs.109.1.199
31. Leal J, Shaner S, Jedrusik N, Savelyeva A, Asplund M. Electrotaxis evokes directional separation of co-cultured keratinocytes and fibroblasts. *Sci Rep*. 2023;13(1):11444. doi:10.1038/s41598-023-38664-y
32. Kalantari K, Mostafavi E, Afifi AM, et al. Wound dressings functionalized with silver nanoparticles: promises and pitfalls. *Nanoscale*. 2020;12 (4):2268–2291. doi:10.1039/C9NR08234D
33. Kukushkina EA, Mateos H, Altun N, et al. Highly Stable Core-Shell Nanocolloids: synergy between Nano-Silver and Natural Polymers to Prevent Biofilm Formation. *Antibiotics*. 2022;11(10). doi:10.3390/antibiotics11101396.
34. Du P, Suhaeri M, Ha SS, Oh SJ, Kim SH, Park K. Human lung fibroblast-derived matrix facilitates vascular morphogenesis in 3D environment and enhances skin wound healing. *Acta Biomater*. 2017;54:333–344. doi:10.1016/j.actbio.2017.03.035
35. Torkaman G. Electrical Stimulation of Wound Healing: a Review of Animal Experimental Evidence. *Adv Wound Care*. 2014;3(2):202–218. doi:10.1089/wound.2012.0409

36. Chen H, Ma X, Zhang M, Liu Z. Injectable and biofunctionalized fibrin hydrogels co-embedded with stem cells induce hair follicle genesis. *Regen Biomater*. 2023;10:rbac086. doi:10.1093/rb/rbac086
37. Holzer-Geissler JCJ, Schwingenschuh S, Zacharias M, et al. The Impact of Prolonged Inflammation on Wound Healing. *Biomedicines*. 2022;10 (4):856. doi:10.3390/biomedicines10040856
38. Krzyszczyk P, Schloss R, Palmer A, Berthiaume F. The Role of Macrophages in Acute and Chronic Wound Healing and Interventions to Promote Pro-wound Healing Phenotypes. *Front Physiol*. 2018;9:419. doi:10.3389/fphys.2018.00419
39. Joorabloo A, Liu T. Recent advances in nanomedicines for regulation of macrophages in wound healing. *J Nanobiotechnology*. 2022;20(1):407. doi:10.1186/s12951-022-01616-1
40. Bao MH, Li GY, Huang XS, Tang L, Dong LP, Li JM. Long Noncoding RNA LINC00657 Acting as a miR-590-3p Sponge to Facilitate Low Concentration Oxidized Low-Density Lipoprotein-Induced Angiogenesis. *Mol Pharmacol*. 2018;93(4):368–375. doi:10.1124/mol.117.110650
41. Zeng G, Wu Z, Cao W, Wang Y, Deng X, Zhou Y. Identification of anti-nociceptive constituents from the pollen of Typha angustifolia L. using effect-directed fractionation. *Nat Prod Res*. 2020;34(7):1041–1045. doi:10.1080/14786419.2018.1539979
42. Yi-Wen Z, Mei-Hua B, Xiao-Ya L, Yu C, Jing Y, Hong-Hao Z. Effects of Oridonin on Hepatic Cytochrome P450 Expression and Activities in PXR-Humanized Mice. *Biol Pharm Bull*. 2018;41(5):707–712. doi:10.1248/bpb.b17-00882
43. Zhang YW, Zheng XW, Liu YJ, et al. Effect of Oridonin on Cytochrome P450 Expression and Activities in HepaRG Cell. *Pharmacology*. 2018;101 (5–6):246–254. doi:10.1159/000486600
44. Gürkan A, Tekdal GP, Bostancı N, Belibasakis GN. Cytokine, chemokine, and growth factor levels in peri-implant sulcus during wound healing and osseointegration after piezosurgical versus conventional implant site preparation: randomized, controlled, split-mouth trial. *J Periodontol*. 2019;90 (6):616–626. doi:10.1002/JPER.18-0216
45. Ley K. M1 Means Kill; M2 Means Heal. *J Immunol*. 2017;199(7):2191–2193. doi:10.4049/jimmunol.1701135
46. Kim SY, Nair MG. Macrophages in wound healing: activation and plasticity. *Immunol Cell Biol*. 2019;97(3):258–267. doi:10.1111/imcb.12236
47. You C, Li Q, Wang X, et al. Silver nanoparticle loaded collagen/chitosan scaffolds promote wound healing via regulating fibroblast migration and macrophage activation. *Sci Rep*. 2017;7(1):10489. doi:10.1038/s41598-017-10481-0
48. Carvalho EO, Fernandes MM, Padrao J, et al. Tailoring Bacteria Response by Piezoelectric Stimulation. *ACS Appl Mater Interfaces*. 2019;11 (30):27297–27305. doi:10.1021/acsami.9b05013
49. Yang AL, Sun SB, Qu LY, et al. Polysaccharide hydrogel containing silver nanoparticle@catechol microspheres with photothermal, antibacterial and anti-inflammatory activities for infected-wounds repair. *Int J Biol Macromol*. 2024;265(Pt 2):130898. doi:10.1016/j.ijbiomac.2024.130898
50. Wang Y, Zhai W, Li J, Liu H, Li C, Li J. Friction behavior of biodegradable electrospun polyester nanofibrous membranes. *Tribol Int*. 2023;188:108891. doi:10.1016/j.triboint.2023.108891
51. Wang Y, Xu Y, Zhai W, et al. In-situ growth of robust superlubricated nano-skin on electrospun nanofibers for post-operative adhesion prevention. *Nat Commun*. 2022;13(1):5056. doi:10.1038/s41467-022-32804-0
52. Yin Y, Guo C, Mu Q, Li W, Yang H, He Y. Dual-sensing nano-yarns for real-time pH and temperature monitoring in smart textiles. *Chem Eng J*. 2024;500:157115. doi:10.1016/j.cej.2024.157115
53. Chen X, Zhao M, Xie Q, et al. Click-hydrogel delivered aggregation-induced emissive nanovesicles for simultaneous remodeling and antibiosis of deep burn wounds. *Aggregate*. 2024;5(1):e406. doi:10.1002/agt2.406